Photocatalysis

DOI: 10.1002/ange.201406625

Molecular-Level Understanding of the Photocatalytic Activity Difference between Anatase and Rutile Nanoparticles**

*Wooyul Kim, Takashi Tachikawa, Gun-hee Moon, Tetsuro Majima, and Wonyong Choi**

Abstract: *The generation of oxidants on illuminated photocatalysts and their participation in subsequent reactions are the main basis of the widely investigated photocatalytic processes for environmental remediation and selective oxidation. Here, the generation and the subsequent diffusion of ·OH from the illuminated TiO_2 surface to the solution bulk were directly observed using a single-molecule detection method and this molecular phenomenon could explain the different macroscopic behavior of anatase and rutile in photocatalysis. The mobile ·OH is generated on anatase but not on rutile. Therefore, the photocatalytic oxidation on rutile is limited to adsorbed substrates whereas that on anatase is more facile and versatile owing to the presence of mobile ·OH. The ability of anatase to generate mobile ·OH is proposed as a previously unrecognized key factor that explains the common observations that anatase has higher activity than rutile for many photooxidative reactions.*

Semiconductor photocatalysis is a key chemical process for solar energy utilization. It is mediated by the photoinduced charge transfers occurring on the semiconductor/water (or air) interface, which is often accompanied by the generation of reactive radical species such as the hydroxyl radical and superoxides.[1] In particular, the generation of the OH radical (·OH) on UV-illuminated TiO_2 surface is a key step in the intensively studied photocatalysis for the purification of polluted water and air. Although the involvement of OH radicals in the photocatalytic process is widely accepted, the nature of the reaction mechanism is complex and not clearly understood because the photocatalytic activities of TiO_2 are often specific for the substrate and for the catalyst sample used.[2] The photocatalytic degradation of pollutants using UV-illuminated TiO_2 (one of the most frequently and thoroughly studied photoactive materials) has been successfully demonstrated for an immense number of substrates, which is largely ascribed to the strong oxidation potential of the photogenerated valence band (VB) holes and OH radicals (free, $\cdot OH_f$, or surface bound, $\cdot OH_s$).[1,2] The photochemical generation and behavior of reactive oxygen species (ROS) is vitally important in determining the photocatalytic activity of TiO_2 but not much is known regarding this critical process at the molecular level.

In photocatalytic oxidation processes, the hole and $\cdot OH_s$ react mainly with adsorbed substrates and the desorption of intermediates from the surface should inhibit further mineralization. On the other hand, mobile $\cdot OH_f$ can react with both surface-bound and unbound substrates/intermediates and is a more versatile oxidant. Although $\cdot OH_f$ is believed to be generated in the TiO_2 photocatalytic reaction,[3] previous studies addressed the desorption of $\cdot OH_f$ at the TiO_2/air interface[4] and there has been no direct evidence supporting the diffusion of $\cdot OH_f$ from the illuminated TiO_2 surface in water. This study demonstrated the existence of the diffusing $\cdot OH_f$ in aqueous medium for the first time using a single-molecule detection technique based on total internal reflection fluorescence microscopy (TIRFM).[4f,5] The observed molecular behavior of OH radicals and their role in the macroscopic photocatalysis were investigated for the model photocatalysis system employing anatase and rutile nanoparticles in water. Why anatase and rutile forms of titania exhibit different photocatalytic activities has been an important and frequently raised question. Although it has been frequently dealt with,[6–11] here we propose a new view based on the molecular behavior of photogenerated OH radicals. The $\cdot OH_f$ diffusing from the irradiated anatase TiO_2 into the aqueous bulk was observed, whereas this behavior was not observed with rutile. The molecular events occurring on irradiated TiO_2 nanoparticles (anatase and rutile) and the macroscopic photocatalytic behavior in bulk slurry systems can be successfully correlated.

It has been often reported that the activities of anatase TiO_2 are higher than those of rutile TiO_2 for various photocatalytic reactions.[6] Although the higher photoactivity of anatase has been ascribed to a wider band gap,[7] slower charge recombination kinetics,[8] higher charge carrier mobility,[9] deeper excitation of charge carriers in bulk,[10] and the different kinds of photogenerated ROS,[11] there is lack of clear understanding. In most of the previous photocatalytic studies that compared anatase and rutile, their properties such as the surface area, particle size, and the level of defects are significantly different and therefore, the observed activity

[*] Dr. W. Kim, G.-h. Moon, Prof. W. Choi
School of Environmental Science and Engineering
Pohang University of Science and Technology (POSTECH)
Pohang, 790-784 (Republic of Korea)
E-mail: wchoi@potech.edu
Prof. T. Tachikawa,[+] Prof. T. Majima
The Institute of Scientific and Industrial Research (SANKEN)
Osaka University, Mihogaoka 8-1, Ibaraki
Osaka, 567-0047 (Japan)
[+] Present address: Department of Chemistry, Graduate School of Science, Kobe University, 1 – 1 Rokkodai-cho, Nada-ku, Kobe 657 – 8501 (Japan)

[**] This work was supported by the Global Frontier R&D Program on the Center for Multiscale Energy System (No. 2011-0031571), and KCAP (Sogang University) (No. 2009-0093880) funded by the Korea government (MSIP) through NRF. We acknowledge Dr. Narayanan Lakshminarasimhan for XRD analysis.

Supporting information for this article is available on the WWW under http://dx.doi.org/10.1002/anie.201406625.

difference cannot be ascribed solely to the intrinsic difference of the crystalline phase. To minimize the interferences from other intrinsic properties, in this study, pure anatase and rutile samples were obtained by the selective etching of P25 TiO_2 (having mixed crystallinity).[12] Since both anatase and rutile samples were derived from the same parent particles (P25), their physicochemical properties are not very different as apparent in Table 1. Powder X-ray diffractograms and diffuse reflectance spectra confirmed that each etched phase is pure anatase and rutile (Figures S1 and S2). The distribution of particle sizes was analyzed from transmission electron microscopy (TEM) images (of up to 500 particles, Figure S3) and the average size of particles observed by TEM closely matches with that calculated from the Debye–Scherrer equation (Table 1).

Table 1: Properties of anatase and rutile etched from P25 TiO_2.

TiO_2 phase	BET surface area [$m^2 g^{-1}$]	Crystallite size [nm][a]	Hydrodynamic size [nm][b]	Particle size [nm][c]	Zeta potential [mV][d]
anatase	62	22	236	21	35 (±5)
rutile	31	34	193	35	42 (±3)

[a] Calculated from XRD and the Debye–Scherrer equation. [b] Measured by an electrophoretic light scattering spectrometer. [c] Measured by TEM, averaging at least 500 particles. [d] Measured at pH 3.

To directly monitor the behavior of $^{\bullet}OH_f$ diffusing from the surface of anatase and rutile to water medium, the previous experimental setup (TIRFM) for detecting air-born OH radicals[4f] was modified as shown in Scheme 1. HPF (3′-(*p*-hydroxyphenyl)fluorescein) selectively reacts with $^{\bullet}OH$ (but not with $O_2^{\bullet-}$, $^1O_2$, and H_2O_2 generated on UV-irradiated TiO_2) and transforms into a strongly fluorescing product.[13] Therefore, HPF was used for the selective single-molecule detection of $^{\bullet}OH_f$ under experimental condition in which HPF was not in direct contact with the TiO_2 surface. In this work, to detect $^{\bullet}OH_f$ in water, HPF was modified with a silylated group as an anchor that prevents detachment from a cover glass (Figure S4). When the underivatized HPF coated on the cover glass was used, most HPF molecules desorbed from the surface and little fluorescence signal was observed (Figure S5). Figure 1 a–d show the single-molecule fluorescence images observed before and after UV irradiation of the anatase and rutile films for 5 s in water and 2 s in air, respectively. After UV irradiation, bright fluorescent signals clearly emerged over the irradiated region of the anatase film, whereas the signals generated over rutile were negligible. The fluorescent signals may not be directly comparable between the water and air systems since the number of HPF molecules on the cover glass (in air/TiO_2 case) might be different from that of silylated HPF (in water/TiO_2). However, the observation that the signals in anatase/water (Figure 1 a) are localized within the UV-irradiated region (yellow circles) compared with those of the anatase/air system (Figure 1 c) [despite the longer UV-irradiation time (5 s) and the shorter diffusion distance (7.5 μm) in the anatase/water system] indicates that the water-born $^{\bullet}OH_f$ is much short-lived and less mobile than air-born $^{\bullet}OH_f$. All fluorescence experiments were repeated 3–10 times over different regions to confirm the reproducibility (Table S1). The fluorescence signals were completely quenched in the presence of DMSO as an $^{\bullet}OH$ scavenger, which excludes the possibility that signals may originate from any fluorescing impurities.

The total amount of $^{\bullet}OH$ (without distinction between $^{\bullet}OH_s$ and $^{\bullet}OH_f$) was also monitored in steady-state photocatalysis of a TiO_2 slurry by three different methods (Figure 2 a and Figure S6). Benzoic acid (BA),[14] coumarin,[15] and HPF[13] were used as probe molecules for $^{\bullet}OH$ detection and their oxidized products (generated as a result of the reaction with $^{\bullet}OH$) were quantified by HPLC chromatography (for *p*-hydroxybenzoic acid, *p*-HBA) and fluorescence spectroscopy (for 7-hydroxycoumarin and fluorescein). Regardless of the test method, a similar trend of $^{\bullet}OH$ production activity (anatase ≫ rutile) was observed, which supports the previous reports.[6c,d,11b,c] Although the single molecule fluorescence image analysis showed the absence of $^{\bullet}OH_f$ on rutile (Figure 1 b), the production of $^{\bullet}OH$ (i.e., *p*-HBA) on rutile was observed with a reduced activity (Figure 2 a) since *p*-HBA can be generated from the reaction with $^{\bullet}OH_s$. To differentiate the reaction of $^{\bullet}OH_s$ from that of $^{\bullet}OH_f$, the production of *p*-HBA was compared between bare TiO_2 and Nafion-coated TiO_2 slurry systems (Figure 2 b). Nafion is frequently employed as an inert support of photoactive catalysts, because the perfluorinated polymer itself is stable against photocatalytic oxidation and does not react with ROS.[16] The Nafion layer on anatase and rutile was analyzed to confirm the homogeneity of the surface coverage (Figures S7–S9). When the surface of TiO_2 is coated with Nafion,[16] the direct contact between $^{\bullet}OH_s$ and the substrate (BA) should be inhibited by this barrier and the oxidation of BA should be mediated preferentially by $^{\bullet}OH_f$ (Figure 2 b inset). Figure 2 b shows that the hydroxylation inhibition effects induced by the Nafion layer are very different between the anatase and rutile systems. With a thin Nafion layer (10–20 $mg\,g^{-1}$-TiO_2), the activity of rutile was significantly reduced (by ≈40%) whereas that of anatase was little affected. The Nafion layer may not inhibit the reaction (BA + $^{\bullet}OH_s$) completely because some BA can be absorbed

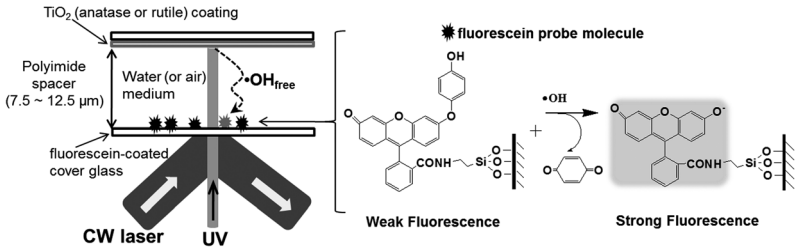

Scheme 1. Illustration of the experimental setup for the single molecule detection of photogenerated $^{\bullet}OH_f$ in water. Anatase or rutile was coated on the upper cover glass and the modified fluorescein (HPF) was anchored on the lower glass through a silanol group. The intervening gap was controlled using polyimide films. The gap was filled with air-saturated water.

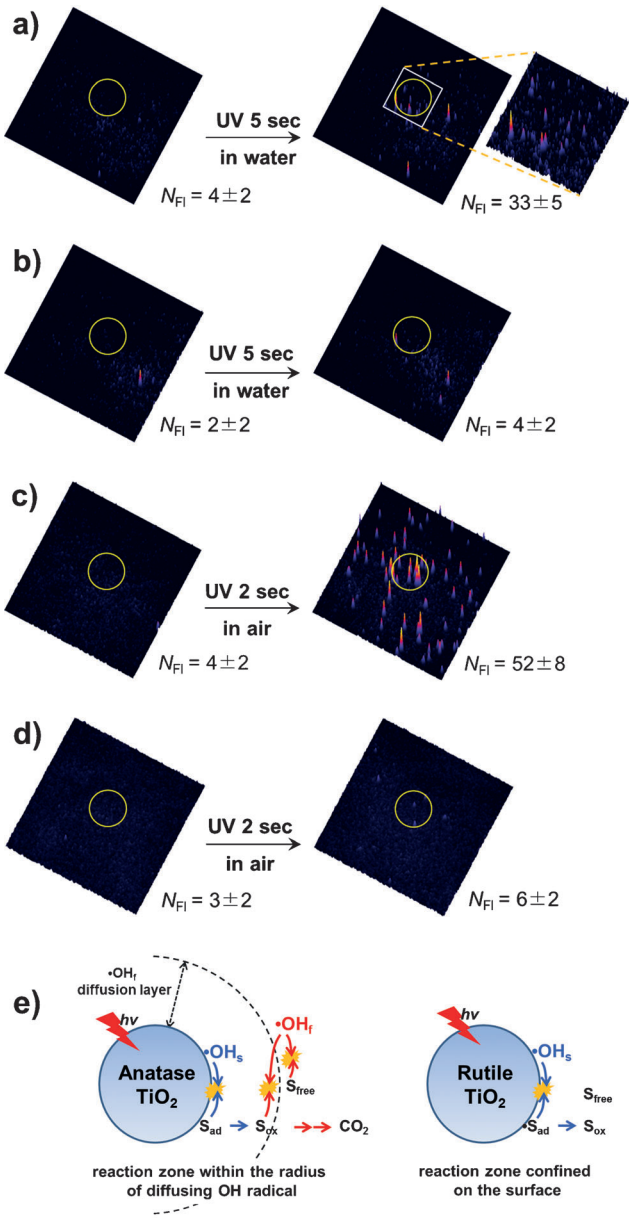

Figure 1. Fluorescence images of •OH$_f$ that migrated through a gap from the UV-illuminated TiO_2 to HPF-coated cover glass. a–d) The TiO_2/water system with silanol-modified HPF [anatase (a) and rutile (b)] and the TiO_2/air system with HPF [anatase (c) and rutile (d)] were compared before (left) and after (right) UV irradiation for 5 s (water) and 2 s (air). The diffusion gap is 7.5 μm (water) and 12.5 μm (air). The UV irradiation region is inside the yellow circle in the images. N_{FI} indicates the number of fluorescence signals. The size of the images is 50×50 μm. e) Illustration of OH-radical-mediated photocatalysis on anatase (left) and rutile (right).

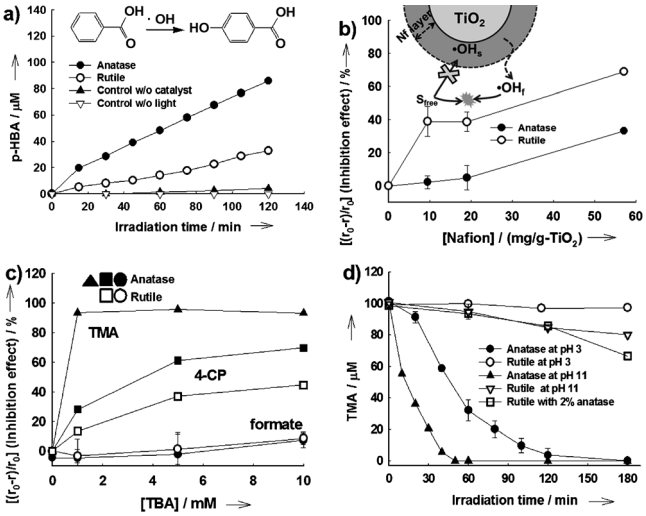

Figure 2. The distinction between •OH$_s$ and •OH$_f$ in the bulk-slurry photocatalytic system. a) Time profiles for the photocatalytic production of *p*-HBA from the oxidation of BA. b) Inhibition of *p*-HBA production by Nafion coating on TiO_2 as a function of Nafion loading. c) Inhibition of pollutant degradation (TMA, 4-CP, and formate) by TBA addition in the suspension of anatase and rutile under UV illumination. TMA on rutile was not degraded at all regardless of the TBA concentration. r_0 and r represent the initial reaction rate (μM min^{-1}) in the absence and presence of Nafion for (b) [or TBA for (c)]. d) The time profiles of TMA degradation in the aqueous suspensions of anatase and rutile are compared between pH 3 and 11. The rutile sample containing 2% of unetched anatase phase is compared as well. Experimental conditions were $[TiO_2]=0.5$ g L^{-1}, $[4\text{-CP}]_0$, $[\text{formate}]_0$, and $[TMA]_0=100$ μM, $[BA]_0=10$ mM, $[TBA]_0=1$, 5, and 10 mM, $pH_i=3$, air saturation, and $\lambda>300$ nm (or $\lambda>320$ nm for 4-CP).

into the Nafion layer. Nevertheless, this indicates that the hydroxylation on rutile is initiated mainly by •OH$_s$ whereas that on anatase is achieved by •OH$_f$ that can diffuse out through the Nafion layer. The fact that the hydroxylation activity of rutile is more sensitively influenced by the presence of the Nafion layer (in macroscopic photocatalysis in water) is consistent with the lack of •OH$_f$ production on rutile (in single-molecule detection).

The role of •OH$_s$ and •OH$_f$ in the photocatalytic oxidation in water was further investigated by monitoring the effect of addition of *tert*-butyl alcohol (TBA; scavenger of •OH) on the photocatalytic degradation of organic substrates in the suspension of anatase and rutile. Three substrates (formate[17] as an anionic substrate, 4-chlorophenol (4-CP)[18] as a neutral substrate, and tetramethylammonium (TMA)[2a,c,3c] as a cationic substrate) were selected because they have different electrostatic interactions with the positively charged TiO_2 surface (at pH 3; Figure 2c). Formate anions should be attracted onto the surface,[17] whereas TMA cations are repelled from the surface.[2a,c,3c] Under such condition, formate is degraded mainly by •OH$_s$ and TMA by •OH$_f$.[2a,c,3c] 4-CP which is not adsorbed on nor repelled from the TiO_2 surface should be degraded by both •OH$_s$ and •OH$_f$. Since TBA little adsorbs on TiO_2 surface, TBA should scavenge •OH$_f$ preferentially. Therefore, the presence of TBA significantly retards the degradation of nonadsorbing substrates, while it has only little effect on the degradation of surface-adsorbed substrates.[19] Figure 2c shows that the TBA-induced inhibition effect is markedly high with TMA and insignificant with formate, which supports that TMA degradation is mediated mainly by •OH$_f$ (in the solution bulk) and formate degradation by •OH$_s$ (on the surface). The TBA inhibition effect was more prominent with anatase than rutile in the cases of TMA and 4-CP degradation, which means that

the contribution from $^{\bullet}OH_f$-mediated oxidation is higher with anatase than rutile. This is also consistent with the fact that rutile shows no activity for the photocatalytic degradation of TMA at pH 3 (degraded by $^{\bullet}OH_f$) (Figure 2d) but measurable activities for 4-CP and formate (degraded by $^{\bullet}OH_s$). The inability of generating $^{\bullet}OH_f$ on rutile, which was confirmed by the single-molecule fluorescence image analysis, explains why rutile cannot degrade TMA at all and why the photocatalytic oxidation on rutile is less affected by the presence of hydroxyl radical scavengers (TBA). It can be concluded that the photocatalytic oxidation is initiated by both $^{\bullet}OH_s$ and $^{\bullet}OH_f$ on anatase (both surface and bulk reactions) whereas it is done mainly by $^{\bullet}OH_s$ on rutile (surface reaction only) (Figure 1e). The pH-dependent photocatalytic activities of TMA degradation with anatase and rutile, which are shown in Figure 2d, are consistent with this conclusion. Although rutile is completely inactive for TMA degradation at pH 3 (at which the electrostatic interaction is repulsive), it shows a non-negligible activity at pH 11 (at which the electrostatic interaction is attractive) because $^{\bullet}OH_s$ generated on rutile can attack TMA molecules. It is interesting to note that even a small fraction of anatase remaining in the etched rutile (rutile with 2% anatase in Figure 2d) induced a measurable degradation of TMA at pH 3. This indicates that the presence of anatase is essential for the photocatalytic degradation of TMA at pH 3, which implies that the diffusing $^{\bullet}OH_f$ generated on anatase are needed to reach the TMA molecules that are repelled from the TiO_2 surface at pH 3. Therefore, the photocatalytic degradation of TMA on anatase at pH 3 was greatly enhanced compared with that on rutile. TMA degradation for anatase at pH 11 was highly enhanced, because the oxidation of TMA was initiated by both $^{\bullet}OH_s$ and $^{\bullet}OH_f$ (both surface and bulk reactions).

Anatase and rutile can be different in their charge recombination dynamics, which may contribute to the different activities. The recombination kinetics in anatase and rutile were compared using time-resolved diffuse reflectance (TDR) spectroscopy. TDR spectra of anatase and rutile show the typical broad absorption band of the trapped holes and electrons in TiO_2 (Figure S7).[20] Figure 3 compares the normalized time traces of absorption at 550 nm (mainly derived from trapped hole) during the 355 nm laser photolysis of anatase and rutile in water. The time-resolved decay at 550 nm was slower in anatase than rutile, which implies a longer lifetime of photogenerated charge carriers and a higher efficiency of ROS generation in anatase.[8] However, the difference in recombination dynamics between anatase and rutile cannot fully explain the difference in their photocatalytic activities as discussed below.

Table 2 compares the initial photocatalytic degradation rates of six test substrates with anatase and rutile at pH 3. Although the activity of anatase is higher than rutile for most cases, the discoloration of AO7 is faster with rutile. Azo dyes can be discolored through various mechanisms (e.g., reaction with various ROS, dye-sensitization path)[2a–e] even in the absence of $^{\bullet}OH_f$ and therefore, AO7 can be discolored on rutile that does not generate $^{\bullet}OH_f$. The activity ratios (A/R) between anatase and rutile are highly substrate-specific, which cannot be simply ascribed to the difference in intrinsic

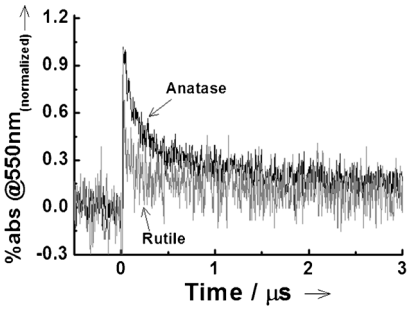

Figure 3. Time-resolved diffuse reflectance spectroscopy measurements. Normalized time traces of absorbance at 550 nm during the 355 nm laser photolysis (1.5 mJ pulse^{-1}) of aqueous suspensions of anatase and rutile TiO_2 nanoparticles in water. The % absorption (%abs) is given by the equation $\%abs = (R_0 - R)/R_0 \times 100$, where R and R_0 represent the intensities of the diffuse reflected monitor light with and without excitation, respectively.

Table 2: Photocatalytic activities of anatase (A) and rutile (R) samples determined with various test substrates.[a]

TiO_2 phase	TMA	DCA	4-CP	EDTA	Cr^{VI}	AO7
A	**1.0**	**23**	**4.4**	**15.6**	**5.9**	1.7
(ads%)	(<1)	(<1)	(<1)	(20)	(22)	(41)
R	0	0.78	0.94	5.6	3.5	**3.9**
(ads%)	(<1)	(<1)	(<1)	(18)	(14)	(11)
activity ratio (**A/R**)	⩾1	29	4.7	2.8	1.7	0.44

[a] The listed numbers represent the initial removal rate (μM min^{-1}). The experimental uncertainty was within ±10%. The most active TiO_2 sample for a given substrate is in bold numbers. The numbers in parenthesis indicate the adsorbed fraction (ads%) of each substrate on anatase and rutile at equilibrium prior to UV irradiation. The experimental conditions were $[TiO_2] = 0.5$ g L^{-1}, $[TMA]_0 = [DCA]_0 = [4\text{-}CP]_0 = [AO7]_0 = 100$ μM, $[EDTA]_0 = 500$ μM, $[Cr^{VI}]_0 = 200$ μM, 300 nm (or $\lambda > 320$ nm for 4-CP), $pH_i = 3$ and air-saturated.

properties of two polymorphs (e.g., bandgap, recombination dynamics, mobility of charge carriers). It is interesting to note that the activity ratios (A/R) are high with nonadsorbing substrates (TMA, DCA, 4-CP) whereas they are generally low with adsorbing substrates (AO7, Cr^{VI}, EDTA). This supports that the photocatalysis of anatase (producing $^{\bullet}OH_f$) is more efficient in oxidizing nonadsorbing substrates than that of rutile (not producing $^{\bullet}OH_f$). Rutile reacts preferentially with adsorbed substrates because its inability to produce $^{\bullet}OH_f$ mainly limits its reaction on the surface region.

The relative roles of $^{\bullet}OH_s$, $^{\bullet}OH_f$, and VB hole can be different in the degradation of each substrate, which may be related to the substrate-specific activity of anatase and rutile. For example, although rutile shows the higher color removal rate (2.3 times), the mineralization process is more efficient with anatase: the total organic carbon (TOC) removal of AO7 in anatase suspension was 84% after 1 h irradiation, whereas that for rutile was 28%. This implies that the initial destruction of the chromophoric group in AO7 can be mediated by VB holes or $^{\bullet}OH_s$, but the further degradation and mineralization require the action of $^{\bullet}OH_f$ that is absent in the rutile system. If the oxidation activity difference between

anatase and rutile is largely ascribed to the behavior of OH radicals, the photocatalytic reduction activity of anatase and rutile might be different from the oxidation counterpart. As for the reductive conversion of hexavalent chromium ($Cr^{VI} \rightarrow Cr^{III}$; Table 2), the activity ratio (A/R) is 1.7. Considering that the specific surface area of anatase is twice as large as that of rutile (Table 1), there is little difference between anatase and rutile in the intrinsic photocatalytic activity (normalized by surface area) for the reductive conversion. A previous study[2a] also reported that the photocatalytic reduction activity of rutile is comparable or even higher than that of anatase for the reduction of Ag^+ on TiO_2. The faster recombination in rutile cannot provide an explanation for this. The common belief that anatase is more active than rutile is not valid for photocatalytic reduction reactions.

In this respect, the electron transfer to O_2 (as an electron acceptor) on anatase and rutile should also be considered. This O_2 reduction part is slow and often limits the overall kinetics of photocatalysis. The efficiency of OH radical photogeneration in the suspension of anatase and rutile was compared (by using the coumarin method) in air and O_2-saturated condition (Figure S11). Higher O_2 concentration (under O_2 saturation) enhanced the hydroxylation of coumarin on rutile more than on anatase (the enhancement factor (O_2 versus air saturation) is 1.96 and 1.25 for rutile and anatase, respectively), which indicates that the OH radical production on rutile is more limited by the O_2 reduction part than that on anatase. The conduction band (CB) edge potential of rutile is slightly more positive (by 0.1–0.2 V) than that of anatase. Therefore, the hindered formation of $^{\bullet}OH_f$ on rutile might be related to the inefficiency of the reductive pathway of OH radical generation[1e] (i.e., the path of $O_2 \rightarrow H_2O_2 \rightarrow {}^{\bullet}OH$). According to our preliminary test, the formation of $^{\bullet}OH_f$ is negligible in the presence of Ag^+ (stronger CB electron scavenger than O_2) that should hinder the reduction of O_2, implying that the reductive pathway can be responsible for $^{\bullet}OH_f$ formation. That is, not only the VB hole-mediated path but also the CB electron-mediated path may contribute to the generation of $^{\bullet}OH_f$. A more detailed study of the mechanism of $^{\bullet}OH_f$ formation on anatase and rutile is under investigation. Although the photocatalytic activities of anatase and rutile can be influenced by many parameters such as the width and position of the band gap,[7,21] and the charge recombination dynamics and mobility of charge carriers,[8–10] this study newly proposes, on the basis of the molecular level observation and its relation with the slurry-phase photocatalysis, that the photogeneration of $^{\bullet}OH_f$ is preferred on anatase, not rutile and that the action of $^{\bullet}OH_f$ is critical in determining the overall photocatalytic oxidation activity. Considering that the majority of photocatalytic applications are related to the oxidative conversion, the present finding provides new insight for understanding photocatalysis behaviors and mechanisms.

In summary, the diffusion of $^{\bullet}OH_f$ from the illuminated TiO_2 surface into the aqueous solution was for the first time directly observed using a single-molecule detection system. The generation of diffusing $^{\bullet}OH_f$ was clearly observed on anatase but not on rutile. The diffusion of $^{\bullet}OH_f$ from the surface into the aqueous bulk greatly extends the reaction zone and makes the photocatalytic oxidation reaction not only heterogeneous (occurring only on the surface) but also homogeneous (occurring in the solution bulk) in its nature. However, the photocatalytic reaction zone on rutile that cannot generate $^{\bullet}OH_f$ is limited mainly to the surface, which makes the oxidation and mineralization of nonadsorbing substrates and intermediates less efficient. The fact that the photocatalytic activities of anatase and rutile are highly substrate-specific, which cannot be explained in terms of the different properties of the titanium material itself (e.g., different band gap, band edge position, and charge recombination dynamics), can be understood on the basis of the different behavior of OH radicals generated on anatase and rutile and the different adsorption properties of substrates (and their degradation intermediates) on anatase and rutile. In particular, the photogeneration of $^{\bullet}OH_f$ is critical in achieving the mineralization of nonadsorbing substrates. The common observation that an anatase photocatalyst is more active than rutile is now attributed to the facile generation of $^{\bullet}OH_f$ on anatase. Although the photocatalytic activity difference between anatase and rutile cannot be ascribed solely to the molecular behavior of $^{\bullet}OH_f$, it is an important factor which has not been recognized before. However, the fundamental question of why anatase allows the desorption of $^{\bullet}OH_f$ and rutile does not remain unanswered. Further experimental and theoretical studies are underway to gain a molecular-level understanding of this phenomenon.

Received: June 26, 2014
Published online: October 14, 2014

Keywords: anatase · hydroxyl radicals · photocatalysis · rutile · TiO_2

[1] a) M. R. Hoffmann, S. T. Martin, W. Choi, D. W. Bahnemann, *Chem. Rev.* **1995**, *95*, 69–96; b) A. L. Linsebigler, G. Lu, J. T. Yates, *Chem. Rev.* **1995**, *95*, 735–758; c) A. Fujishima, T. N. Rao, D. A. Tryk, *J. Photochem. Photobiol. C* **2000**, *1*, 1–21; d) P. Salvador, *J. Phys. Chem. C* **2007**, *111*, 17038–17043; e) V. Diesen, M. Jonsson, *J. Phys. Chem. C* **2014**, *118*, 10083–10087.

[2] a) J. Ryu, W. Choi, *Environ. Sci. Technol.* **2008**, *42*, 294–300; b) H. Park, Y. Park, W. Kim, W. Choi, *J. Photochem. Photobiol. C* **2013**, *15*, 1–20; c) W. Kim, J. Park, H. J. Jo, H.-J. Kim, W. Choi, *J. Phys. Chem. C* **2008**, *112*, 491–499; d) C. Chen, W. Ma, J. Zhao, *Chem. Soc. Rev.* **2010**, *39*, 4206–4219; e) S. Bae, S. Kim, S. Lee, W. Choi, *Catal. Today* **2014**, *224*, 21–28; f) O. O. Prieto-Mahaney, N. Murakami, R. Abe, B. Ohtani, *Chem. Lett.* **2009**, *38*, 238–239.

[3] a) C. Minero, G. Mariella, V. Maurino, E. Pelizzetti, *Langmuir* **2000**, *16*, 2632–2641; b) C. Minero, G. Mariella, V. Maurino, D. Vione, E. Pelizzetti, *Langmuir* **2000**, *16*, 8964–8972; c) S. Kim, W. Choi, *Environ. Sci. Technol.* **2002**, *36*, 2019–2025.

[4] a) M. C. Lee, W. Choi, *J. Phys. Chem. B* **2002**, *106*, 11818–11822; b) J. S. Park, W. Choi, *Langmuir* **2004**, *20*, 11523–11527; c) Y. Murakami, E. Kenji, A. Y. Nosaka, Y. Nosaka, *J. Phys. Chem. B* **2006**, *110*, 16808–16811; d) Y. Murakami, K. Endo, I. Ohta, A. Y. Nosaka, A. Y. Nosaka, *J. Phys. Chem. C* **2007**, *111*, 11339–11346; e) W. Kubo, T. Tetsuma, *J. Am. Chem. Soc.* **2006**, *128*, 16034–16035; f) T. Tachikawa, T. Majima, *Chem. Soc. Rev.* **2010**, *39*, 4802–4819.

[5] a) T. Funatsu, Y. Harade, M. Tokunaga, K. Saito, T. Yanagida, *Nature* **1995**, *374*, 555–559; b) X. H. Xu, E. S. Yeung, *Science*

1997, *275*, 1106 – 1109; c) K. P. F. Janssen, G. De Cremer, R. K. Neely, A. V. Kubarev, J. Van Loon, J. A. Martens, D. E. De Vos, M. B. J. Roeffaers, J. Hofkens, *Chem. Soc. Rev.* **2014**, *43*, 990 – 1006; d) T. Tachikawa, S. Yamashita, T. Majima, *Angew. Chem. Int. Ed.* **2010**, *49*, 432 – 435; *Angew. Chem.* **2010**, *122*, 442 – 445; e) T. Tachikawa, N. Wang, S. Yamashita, S.-C. Cui, T. Majima, *Angew. Chem. Int. Ed.* **2010**, *49*, 8593 – 8597; *Angew. Chem.* **2010**, *122*, 8755 – 8759.

[6] a) J. T. Carneiro, T. J. Savenije, J. A. Moulijn, G. Mul, *J. Phys. Chem. C* **2010**, *114*, 327 – 332; b) Q. Sun, Y. Xu, *J. Phys. Chem. C* **2010**, *114*, 18911 – 18918; c) M. Murdoch, G. I. N. Waterhouse, M. A. Nadeem, J. B. Metson, M. A. Keane, R. F. Howe, J. Llorca, H. Idriss, *Nat. Chem.* **2011**, *3*, 489 – 492; d) L. Liu, H. Zhao, J. M. Andino, Y. Li, *ACS Catal.* **2012**, *2*, 1817 – 1828.

[7] a) A. Fujishima, X. Zhang, D. A. Tryk, *Surf. Sci. Rep.* **2008**, *63*, 515 – 582; b) L. Kavan, M. Gratzel, S. E. Gilbert, C. Klemenz, J. Scheel, *J. Am. Chem. Soc.* **1996**, *118*, 6716 – 6723.

[8] a) A. Yamakata, T. A. Ishibashi, H. Onishi, *Chem. Phys.* **2007**, *339*, 133 – 137; b) M. Xu, Y. Gao, E. M. Moreno, M. Kunst, M. Muhler, Y. Wang, H. Idriss, C. Wöll, *Phys. Rev. Lett.* **2011**, *106*, 138302.

[9] H. Tang, K. Prasad, R. Sanjines, P. E. Schmid, F. Levy, *J. Appl. Phys.* **1994**, *75*, 2042 – 2047.

[10] T. Luttrell, S. Halpegamage, J. Tao, A. Kramer, E. Sutter, M. Batzill, *Sci. Rep.* **2014**, *4*, 4043.

[11] a) H. Goto, Y. Hanada, T. Ohno, M. Matsumura, *J. Catal.* **2004**, *225*, 223 – 229; b) T. D. Bui, A. Kimura, S. Ikeda, M. Matsumura, *J. Am. Chem. Soc.* **2010**, *132*, 8453 – 8458; c) T. Hirakawa, K. Yawata, Y. Nosaka, *Appl. Catal. A* **2007**, *325*, 105 – 111.

[12] a) T. Ohno, K. Sarukawa, M. Matsumura, *J. Phys. Chem. B* **2001**, *105*, 2417 – 2420; b) B. Ohtani, Y. Azuma, D. Li, T. Ihara, R. Abe, *Trans. Mater. Res. Soc. Jpn.* **2007**, *32*, 401 – 404; c) B. Ohtani, O. O. Prieto-Mahaney, D. Li, R. Abe, *J. Photochem. Photobiol. A* **2010**, *216*, 179 – 182.

[13] K. I. Setsukinai, Y. Urano, K. Kakinuma, H. J. Majima, T. Nagano, *J. Biol. Chem.* **2003**, *278*, 3170 – 3175.

[14] S. H. Joo, A. J. Feitz, D. L. Sedlak, T. D. Waite, *Environ. Sci. Technol.* **2005**, *39*, 1263 – 1268.

[15] K. Ishibashi, A. Fujishima, T. Watanabe, K. Hashimoto, *Electrochem. Commun.* **2000**, *2*, 207 – 210.

[16] a) W. Kim, T. Seok, W. Choi, *Energy Environ. Sci.* **2012**, *5*, 6066 – 6070; b) M. Hara, T. E. Mallouk, *Chem. Commun.* **2000**, 1903 – 1904; c) H. Park, W. Choi, *J. Phys. Chem. B* **2005**, *109*, 11667 – 11674; d) R. Brimblecombe, A. Koo, G. C. Dismukes, G. F. Swiegers, L. Spiccia, *J. Am. Chem. Soc.* **2010**, *132*, 2892 – 2894; e) R. K. Hocking, R. Brimblecombe, L.-Y. Chang, A. Singh, M. H. Cheah, C. Glover, W. H. Casey, L. Spiccia, *Nat. Chem.* **2011**, *3*, 461 – 466.

[17] a) T. Berger, J. M. Delgado, T. Lana-Villarreal, A. Rodes, R. Gomez, *Langmuir* **2008**, *24*, 14035 – 14041; b) M. David, D. M. Savory, A. J. McQuillan, *J. Phys. Chem. C* **2013**, *117*, 23645 – 23656.

[18] F. A. Carey, *Organic Chemistry*, McGraw-Hill, New York, **2000**, p. 676.

[19] J. Kim, C. W. Lee, W. Choi, *Environ. Sci. Technol.* **2010**, *44*, 6849 – 6854.

[20] a) W. Kim, T. Tachikawa, T. Majima, W. Choi, *J. Phys. Chem. C* **2009**, *113*, 10603 – 10609; b) W. Kim, T. Tachikawa, H. Kim, N. Lakshminarasimhan, P. Murugan, H. Park, T. Majima, W. Choi, *Appl. Catal. B* **2014**, *147*, 642 – 650.

[21] D. O. Scanlon, C. W. Dunnill, J. Buckeridge, S. A. Shevlin, A. J. Logsdail, S. M. Woodley, C. R. A. Catlow, M. W. Powell, R. G. Palgrave, I. P. Parkin, G. W. Watson, T. W. Keal, P. Sherwood, A. Walsh, A. A. Sokol, *Nat. Mater.* **2013**, *12*, 798 – 801.

